DOI:10.1021/jf9022146

JOURNAL OF AGRICULTURAL AND FOOD CHEMISTRY
ARTICLE

# Dissolution Mechanism of Crystalline Cellulose in $H_3PO_4$ As Assessed by High-Field NMR Spectroscopy and Fast Field Cycling NMR Relaxometry

Pellegrino Conte,*,† Antonella Maccotta,‡ Claudio De Pasquale,† Salvatore Bubici,§ and Giuseppe Alonzo†

†Dipartimento di Ingegneria e Tecnologie Agro-Forestali (DITAF), Università degli Studi di Palermo, v.le delle Scienze 13, edificio 4, 90128 Palermo, Italy, ‡Dipartimento di Fisica e Tecnologie Relative (DiFTeR), Università degli Studi di Palermo, v.le delle Scienze 13, edificio 18, 90128 Palermo, Italy, and §INVENTO s.r.l., via Nizza 52, 10126 Torino, Italy

Many processes have been proposed to produce glucose as a substrate for bacterial fermentation to obtain bioethanol. Among others, cellulose degradation appears as the most convenient way to achieve reliable amounts of glucose units. In fact, cellulose is the most widespread biopolymer, and it is considered also as a renewable resource. Due to extended intra- and interchain hydrogen bonds that provide a very efficient packing structure, however, cellulose is also a very stable polymer, the degradation of which is not easily achievable. In the past decade, researchers enhanced cellulose reactivity by increasing its solubility in many solvents, among which concentrated phosphoric acid ($H_3PO_4$) played the major role because of its low volatility and nontoxicity. In the present study, the solubilization mechanism of crystalline cellulose in $H_3PO_4$ has been elucidated by using high- and low-field NMR spectroscopy. In particular, high-field NMR spectra showed formation of direct bonding between phosphoric acid and dissolved cellulose. On the other hand, molecular dynamics studies by low-field NMR with a fast field cycling (FFC) setup revealed two different $H_3PO_4$ relaxing components. The first component, described by the fastest longitudinal relaxation rate ($R_1$), was assigned to the $H_3PO_4$ molecules bound to the biopolymer. Conversely, the second component, characterized by the slowest $R_1$, was attributed to the bulk solvent. The understanding of cellulose dissolution in $H_3PO_4$ represents a very important issue because comprehension of chemical mechanisms is fundamental for process ameliorations to produce bioenergy from biomasses.

**KEYWORDS: Fast field cycling NMR; NMRD profile; $^{13}C$ NMR; $^{31}P$ NMR; cellulose; biomasses**

## INTRODUCTION

Cellulose is the most common worldwide distributed biopolymer, and it is also considered as a renewable resource. In fact, it is continuously replenished by the sunlight-catalyzed photosynthetic reduction of $CO_2$ at a velocity comparable to or even faster than its consumption through human activities (*1*). For this reason, it has attracted great attention for the possibility of its use as an inexpensive source of glucose, which, in turn, can be used to achieve bioethanol to be applied as fuel in transport industries (*1*).

Bioethanol can be obtained through fermentation of sugar biomasses (*2*). However, the main criticisms against bioethanol from natural biomasses are related to the reduction of agricultural areas assigned to food crops and enhancement of food costs (*3*, *4*). The possible use of waste materials such as waste paper, cotton-based waste textiles (*5*), flax shivers (*6*), and other lignocellulose materials (*7*) appears to be very suitable. In particular, waste paper, probably one of the most abundant waste materials (*8*, *9*), is considered to be the main resource for obtaining bioethanol not only from enzymatic degradations but also through chemical decays, the mechanisms of which are still uncertain (*10*−*20*).

As is widely known, waste papers are made mainly of cellulose, which is a polysaccharide consisting of a linear chain of several hundreds to over tens of thousands of D-(+)-glucose units linked by $\beta(1\rightarrow4)$-glycosidic bonds. Each D-(+)-glucose unit contains three hydroxyl groups, which can form complex spatial networks of inter- and intramolecular hydrogen bonds. In plant-derived wastes, however, cellulose is also contaminated by lignins and hemicellulose. Due to the complexity of such a biopolymeric network, cellulose is not only resistant to degradation but is also insoluble in all common solvents.

Reliable mechanisms for cellulose degradation should pass through its solubilization. In fact, as for all chemical processes, linkage breaking can be better achieved in single-phase reactions rather than in polyphasic ones (*21*).

Many investigations have been carried out to find the proper solvents for cellulose dissolution (*22*−*30*). Currently, it is known that cellulose can be dissolved in several solvent mixtures, which include heavy metal−amine complex solutions, concentrated metal salts, thiocyanate/amine, lithium chloride/dimethylacetamide,

*Corresponding author (e-mail pellegrino.conte@unipa.it; telephone 00390917028145; fax 0039091484035).

 Published on Web 09/21/2009 

*N*-methylmorphine-*N*-oxide/water, cold sodium hydroxide solutions, and concentrated sulfuric and phosphoric acids. However, in recent years, dissolution in $H_3PO_4$ has been increasingly considered to be a simple and economic method of cellulose pretreatment before its degradation to glucose units (*31*).

To the best of our knowledge, no papers in the literature deal with the mechanisms of cellulose dissolution in phosphoric acid. The aim of the present study was, hence, the recognition of such a mechanism which can be used to optimize the industrial processes involved in ethanol production (*31*, *32*).

## MATERIALS AND METHODS

**Samples.** Crystalline cellulose with 98% purity (CAS Registry No. 9004-34-6) was purchased from Sigma and used without further purification. Its crystallinity degree was 58% as measured by cross-polarization magic angle spinning (CPMAS) $^{13}C$ NMR spectroscopy (see the Supporting Information). Cellulose was dissolved (0.2 g $mL^{-1}$) in 85% $H_3PO_4$ (CAS Registry No. 7664-38-2), also purchased from Sigma, by stirring at 80 °C for 5 min into an oil bain-marie. The cellulose−$H_3PO_4$ solution was used for all NMR analyses without any other treatment. All liquid samples were not degassed.

**High-Field NMR Measurements and Data Elaboration.** $^1H$, $^{31}P$, and $^{13}C$ NMR spectra were acquired with a Bruker Avance II spectrometer equipped with a 5 mm standard bore broadband inverse (BBI) probe operating at 400 MHz on $^1H$, 100 MHz on $^{13}C$, and 162 MHz on $^{31}P$. All of the spectra were acquired with 16K points, a recycle delay of 5 s, a scan number of 5000, an acquisition time of 25 ms, and $^1H$, $^{13}C$, and $^{31}P$ 90° pulses. The $^1H$ 90° pulse was 5 $\mu$s at an attenuation level of −0.4 dB. The $^{13}C$ 90° pulse length was 13 $\mu$s with an attenuation level of −1 dB. The $^{31}P$ 90° pulse length was 16 $\mu$s with an attenuation level of 3.3 dB.

Bruker Topspin 2.0 software was used for spectra acquisition, whereas Mestre-C software (version 4.9.9.9, Mestrelab Research, Santiago de Compostela, Spain) was applied for spectra elaboration. All of the spectra were FT transformed by applying a zero filling with 16K points and no line broadening. Moreover, an automatic baseline correction with Bernstein algorithm was also applied. Chemical shifts were referenced to the resonance of deuterated chloroform at 7.26 ppm for $^1H$ NMR spectra and at 77.36 ppm for $^{13}C$ spectrum and to the signal of 85% orthophosphoric acid at 0 ppm for the $^{31}P$ NMR spectrum. Deuterated chloroform was used as external standard for locking and shimming, thereby avoiding dilution of the solutions with the organic solvent. All of the assignments were done by comparison with literature data.

**FFC-NMR Experiments.** A summary on the theoretical background of fast field cycling NMR relaxometry is reported in the Supporting Information and in the references therein.

$^1H$ NMRD profiles (i.e., relaxation rates $R_1$ or $1/T_1$ vs proton Larmor frequencies) were acquired on a Stelar Spinmaster-FFC-2000 Fast-Field-Cycling Relaxometer (Stelar s.r.l., Mede, PV, Italy) at a constant temperature of 298 K. The proton spins were polarized at a polarization field ($B_{POL}$) corresponding to a proton Larmor frequency ($\omega_L$) of 25 MHz for a period of polarization ($T_{POL}$) of 1 s. The longitudinal magnetization evolution was recorded at values of a relaxation magnetic field ($B_{RLX}$) corresponding to $\omega_L$ comprised in the range of 390−9110 kHz for a period of time ($\tau$) arrayed with 128 values (see the Supporting Information), chosen in an exponential progression from 2.3 to 233 ms. The exponential progression ensured the covering of the entire relaxation curve of interest. Finally, a $^1H$ 90° pulse was used at the starting of the acquisition period contemporarily to an acquisition magnetic field ($B_{ACQ}$) corresponding to a $\omega_L$ of 16.2 MHz. The observable magnetization was revealed as free induction decay (FID) with a time domain of 100 $\mu$s sampled with 512 points. Two scans were accumulated.

The decay curves at each $B_{RLX}$ value (i.e., $^1H$ signal intensity vs $\tau$) were fitted by using either a first-order (eq 1) or a second-order (eq 2) exponential decay function after exportation of the experimental data to OriginPro 7.5 SR6 (version 7.5885, OriginLab Corp., Northampton, MA):

$$I(\tau) = I_0 + A_1 \exp(-\tau/T_1) \quad (1)$$

$$I(\tau) = I_0 + A_1 \exp(-\tau/T_{1a}) + A_2 \exp(-\tau/T_{1b}) \quad (2)$$

In eqs 1 and 2, $I(\tau)$ is the $^1H$ signal intensity at the fixed $B_{RLX}$, $I_0$ is the $^1H$ signal intensity at the thermal equilibrium, $A_i$ is the fitting constant related to the amount of the $i$ nucleus relaxing at $T_{1i}$, and $T_{1i}$ is the $i$th proton spin−lattice relaxation time.

The NMRD profiles reporting the calculated $R_1$ values versus $\omega_L$ were exported to OriginPro 7.5 SR6 and fitted with a Lorentzian function of the type (*33*, *34*)

$$R_1 = A(\omega_0/(4\omega_L{}^2+\omega_0{}^2)) \quad (3)$$

In eq 3, $R_1$ is the longitudinal relaxation time, $\omega_L$ is the proton Larmor frequency, and $A$ is a constant containing the proton quantum-spin number, the proton magnetogyric ratio, the Planck constant, and the electron−nuclear hyperfine coupling constant describing interactions between resonant protons and unpaired electrons. As a matter of fact, the larger this constant, the faster is the longitudinal relaxation rate due to stronger electron−nucleus interactions. $\omega_0$ provides the correlation time ($\tau_c$) through eq 4.

$$\tau_c = 1/\omega_0\pi \quad (4)$$

$\tau_c$ measures the time needed for molecular reorientation, and it is a typical parameter for spectral density which, in turn, describes random molecular motions (*33*). The $\tau_c$ values of all the samples were corrected for the paramagnetic contribution of unpaired electrons (such as those, e.g., in the oxygen gas in the air at equilibrium with all of the liquid solutions) by dividing their value by the $\mu_e/\mu_p$ ratio of 658.21 (*35*). $\mu_e$ is the magnetic moment of the unpaired electrons, whereas $\mu_p$ is that of the protons which were the target nuclei of the present study.

## RESULTS AND DISCUSSION

Dissolution of crystalline cellulose in concentrated $H_3PO_4$ was proved by $^{13}C$ NMR spectroscopy. In fact, **Figure 1** revealed a $^{13}C$ NMR signal pattern similar to that reported in many studies where cellulose dissolution was obtained in solvents or solvent mixtures different from that used in the present study (*24*, *28*, *36*, *37*). Five major peaks at 102, 78, 74, 69, and 61 ppm were observed (**Figure 1**). They were assigned to carbons $C_1$, $C_4$, $C_3 + C_5$, $C_2$, and $C_6$, respectively. The other minor signals were attributed to the α and $\beta$ glucose anomers, which can be present as impurities in the bulk cellulose used for the $H_3PO_4$ dissolution.

$^{31}P$ NMR spectra of either concentrated phosphoric acid (**Figure 2A**) or cellulose in $H_3PO_4$ (**Figure 2B**) revealed a very intense signal at around 0 ppm assigned to the phosphorus in the bulk orthophosphoric acid. The other signals at 11, 6, and −12 ppm were imputable to free monohydrogen and dihydrogen orthophosphates (11 and 6 ppm, respectively) and to polyphosphate chains (−12 ppm).

After cellulose dissolution, a new signal at −2 ppm appeared in the spectrum of **Figure 2B**. This resonance was attributed to a $^{31}P$ nucleus in the orthophosphoric acid directly interacting with the cellulose biopolymer. In fact, it is reported that formation of C−O−P bonds may result in a shielding of the $^{31}P$ nucleus with a consequent upfield peak shift (*38*).

The presence of C−O−P interactions, as evidenced from the spectrum in **Figure 2B**, suggests that phosphoric acid penetrates into the three-dimensional network of crystalline cellulose by breaking the H-bonds of the polysaccharide. As a consequence, a swelling of the biopolymeric chains is achieved, thereby causing solubilization of the crystalline cellulose.

**Figure 3A** reports the NMRD profile of concentrated $H_3PO_4$. The longitudinal relaxation rate values ($R_1$) used to obtain the profile were achieved by interpolating the $^1H$ magnetization decays ($^1H$ signal intensity vs $\tau$) with the monoexponential eq 1. In fact, this equation provided the best fitting with the highest coefficients of correlation ($R^2 > 0.998$) (see Figure S1 in the Supporting Information).

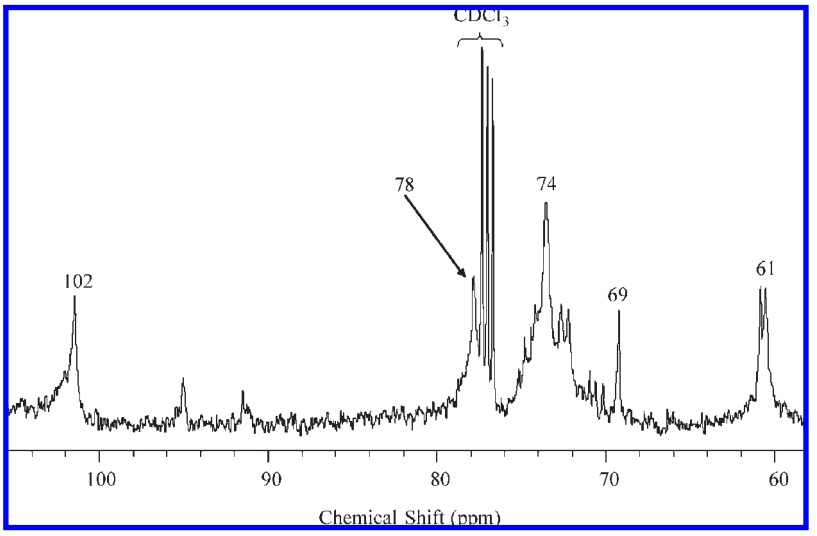


**Figure 1.** $^{13}C$ NMR spectrum of cellulose in phosphoric acid.

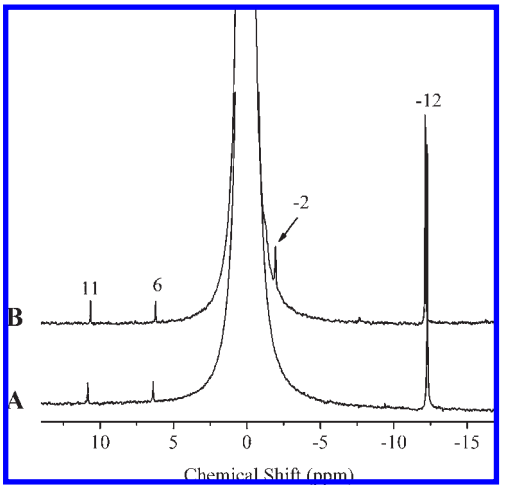


**Figure 2.** $^{31}P$ NMR spectra of concentrated phosphoric acid (**A**) and $H_3PO_4$–cellulose solution (**B**).

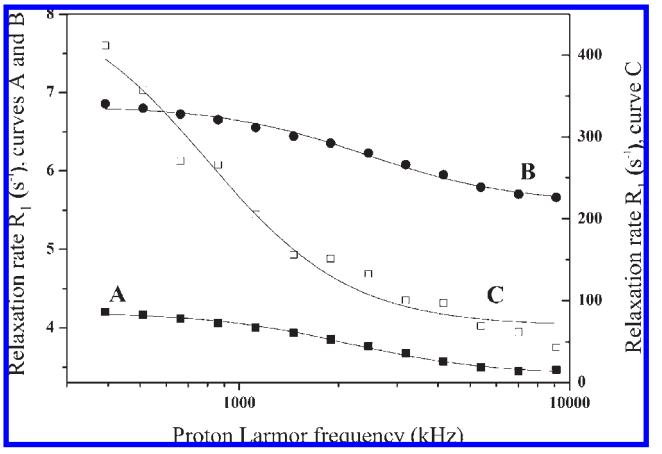


**Figure 3.** NMRD profiles of concentrated $H_3PO_4$ (**A**), bulk phosphoric acid (**B**), and bound $H_3PO_4$ (**C**) in $H_3PO_4$–cellulose solution. The solid lines are the best fittings obtained by applying Lorentzian function.

The NMRD profiles are usually used to retrieve correlation times ($\tau_c$), which, in turn, measure the time needed for molecular reorientation in solution (*39*). $\tau_c$ values are correlated, to a good approximation, either with the molecular weight of polymers or with the aggregate sizes of supramolecular assemblies. As a matter of fact, the shorter the $\tau_c$ values, the smaller are the molecular weights or the sizes of the molecular systems. For this reason, because most of the solvents used in chemical experiments have relatively low molecular weights, it is expected that they provide short correlation times (*40*). In addition, the inverse value of the correlation time ($\tau_c^{-1}$) is also a linear combination of different rates, each representing a time-dependent (TD) process (*34*, *38*). The TD processes affecting $\tau_c^{-1}$ are the electronic relaxation rates, due to the presence of unpaired electrons, the chemical exchange rates, due to solvent–solvent and solute–solvent interactions, and the appropriate rotational rates. All of these factors are also important for the concentrated $H_3PO_4$. For this reason, after fitting the NMRD profile in **Figure 3A** with the monotonic Lorentzian function reported in eq 3 and accounting for the paramagnetic impurities, $\tau_c$ for the pure phosphoric acid was $1.08 \times 10^{-10}$ s, typical for inorganic solvents (*39*, *40*).

In contrast with the $^1H$ signal intensity versus $\tau$ curves obtained for the concentrated $H_3PO_4$, the $H_3PO_4$–cellulose solution revealed decays that were well fitted ($R^2 > 0.998$) by the biexponential eq 2 (see Figure S2 in the Supporting Information).

The biexponentiality of the $H_3PO_4$–cellulose decays was explained by the presence of two different $H_3PO_4$ relaxing components. In particular, according to the results from the high-field NMR spectra, the component that revealed the slowest relaxation rates in the whole $^1H$ $\omega_L$ interval chosen for the present study was due to the bulk $H_3PO_4$ (**Figure 3B**). Conversely, phosphoric acid bound to cellulose yielded the fastest longitudinal relaxations (**Figure 3C**).

The differentiation between the two forms of phosphoric acid was explained by the intensity of the $^1H-^1H$ dipolar interactions. Bulk solvents are not only more mobile than bound ones, but their chemical exchange rates are also more effective. For this reason, the dipolar interactions are weaker in bulk rather than in bound phosphoric acid, thereby enabling slower relaxation mechanisms.

The necessity to assign the two relaxing components to the protons of phosphoric acid in different spatial positions was due to the inability of FFC-NMR spectroscopy to reveal the presence of minor components such as the protons of cellulose. This figure was confirmed by the monodimensional high-field $^1H$ NMR spectrum (**Figure 4**), which showed that the most abundant $^1H$ NMR signal belonged to the phosphoric acid. Signals of cellulose

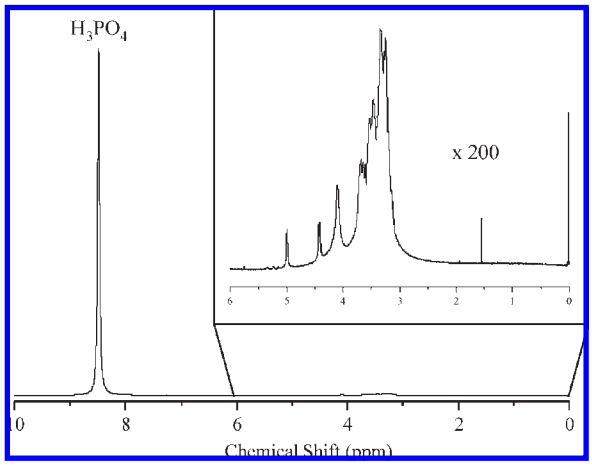


**Figure 4.** $^1$H NMR spectrum of the $H_3PO_4$−cellulose solution. The signal intensity of the $^1$H nuclei in phosphoric acid is 200 times greater than that of cellulose signals evidenced in the square.

were visible only after a ×200 magnification of the $^1$H NMR spectrum baseline (**Figure 4**).

**Figure 3** also shows that all of the longitudinal relaxation rates of the bulk and bound components in $H_3PO_4$−cellulose solution (**Figures 3B**,**C**) were larger than the $R_1$ values measured for the concentrated $H_3PO_4$ (**Figure 3A**). Namely, the $R_1$ values of the bulk $H_3PO_4$ were around 1.7 times larger than those of the pure solvent (compare curves **A** and **B** of **Figure 3**), whereas the longitudinal relaxation rate values appeared to be even larger (from 15 to 100 times more) when the phosphoric acid was bound to the dissolved cellulose (compare curves **A** and **C** of **Figure 3**).

Kimmich and Anoardo (*33*), Lauffer (*34*), and Bakhmutov (*40*) reported that enhancement of relaxation rates can be achieved when interactions between resonating nuclei and unpaired electrons are present in the system. In fact, constant $A$ in eq 3 contains, among others, the electron−nuclear hyperfine coupling constant (see Materials and Methods). The larger this constant, the faster is the longitudinal relaxation rate because of the effect of the coupling between the observed nuclei and the valence-shell electrons. In the present study, it was found that $A_{\text{bound } H_3PO_4} > A_{\text{bulk } H_3PO_4} > A_{\text{pure } H_3PO_4}$, thereby supporting the hypothesis that a larger electronic contribution to the nuclear relaxation arises in $H_3PO_4$ in the order bound > bulk > pure phosphoric acid.

Paramagnetism in $H_3PO_4$−cellulose solution could be generated by the homolytic dissociation of covalent bonds in the rings of the monomer units of cellulose as a consequence of the strong acidic conditions of the solution (pH $<0$). According to this working hypothesis, which still needs to be further verified, the protons of the bound $H_3PO_4$ may experience a stronger effect due to their closest proximity to the paramagnetic centers. Conversely, the bulk phosphoric acid was less affected by the unpaired electrons because of its longer distance from cellulose. However, as stated above, further data must be collected to confirm the paramagnetism of $H_3PO_4$ solutions and the possible effect of negative pH values on the reactivity of dissolved cellulose.

The bound and bulk natures of phosphoric acid in the $H_3PO_4$−cellulose solution were further confirmed by the shapes of the two NMRD profiles (**Figures 3B**,**C**) and by $\tau_c$ evaluations. In particular, it is reported (*40*−*42*) that dispersive-less $R_1$ NMRD profiles of liquid samples (i.e., no or little changes of $R_1$ values with $^1$H $\omega_L$) are associated to non-interacting molecular systems. Conversely, $R_1$ dispersive profiles (i.e., large changes of $R_1$ values with the proton Larmor frequency) are observed when a molecule interacts with other molecular systems in liquids. In this paper, just a little $R_1$ change was observed in the NMRD profile of the relaxing component associated with the bulk $H_3PO_4$ (**Figure 3B**), whereas a $R_1$ variation from a maximum of around 400 $s^{-1}$ down to 50 $s^{-1}$ was observed in the NMRD profile of the component associated with the cellulose-bound phosphoric acid (**Figure 3C**).

Calculation of $\tau_c$ values revealed that the correlation time of the bulk phosphoric acid ($1.03 \times 10^{-10}$ s) was very similar to that of the pure concentrated $H_3PO_4$ ($1.08 \times 10^{-10}$ s), thereby showing that the rotational motions of both systems were similar. On the other hand, the correlation time of the bound phosphoric acid in $H_3PO_4$−cellulose solution was 3 times larger ($3.25 \times 10^{-10}$ s) than that of the bulk component. Because $\tau_c$ is a measure of the time needed for molecular reorientation in solution, it can be concluded that the rate of the rotational motions of the bound phosphoric acid is shortened by the interactions with cellulose.

On the basis of the high- and low-field NMR analyses, a possible dissolution mechanism in concentrated phosphoric acid can be, finally, suggested. Namely, an alteration of the three-dimensional structure of the liquid phosphoric acid in concomitance with the disruption of the microfibrillar structure of cellulose is achieved as a consequence of a solute−solvent reaction. This reaction involves formation of C−O−P bridges between $H_3PO_4$ and cellulose. Therefore, a swelling-like process with a separation of the cellulosic fibrils is obtained. Concomitantly, it is probable that very acidic pH values may favor homolytic resolution of some covalent bonds with a possible increase of the solution paramagnetic properties.

This paper reveals that the combination of high- and low-field NMR spectroscopy can be a powerful tool to retrieve information on reaction mechanisms that are particularly useful for process optimization in biofuel production.

## ACKNOWLEDGMENT

We are grateful to Centro Grandi Apparecchiature − UniNetLab of Università degli Studi di Palermo (http://www.unipa.it/cga/index.html) for having provided machine time at the high-field NMR spectrometer.

**Supporting Information Available:** Acquisition parameters and elaboration details of CPMAS $^{13}$C NMR spectrum of cellulose, theoretical FFC-NMR background, cellulose CPMAS $^{13}$C NMR spectrum and decay curves of concentrated $H_3PO_4$ and $H_3PO_4$−cellulose solution. This material is available free of charge via the Internet at http://pubs.acs.org.

## LITERATURE CITED

(1) Balat, M.; Balat, H.; Öz, C. Progress in bioethanol processing. *Prog. Energ. Combust. Sci.* **2008**, *34*, 551–573.
(2) Kuo, C.; Lee, C. Enhanced enzymatic hydrolysis of sugarcane bagasse by *N*-methylmorpholine-*N*-oxide pretreatment. *Biores. Technol.* **2009**, *100*, 866–871.
(3) Demirbas, A. Biofuels sources, biofuel policy, biofuel economy and global biofuel projections. *Energy Conv. Manage.* **2008**, *49*, 2106–2116.
(4) Pimentel, D.; Marklein, A.; Toth, M. A.; Karpoff, M. N.; Paul, G. S.; McCormack, R.; Kyriazis, J.; Krueger, T. Food versus biofuels: environmental and economic costs. *Hum. Ecol.* **2009**, *37*, 1–12.
(5) Jeihanipour, A.; Taherzadeh, M. J. Ethanol production from cotton-based waste textiles. *Bioresour. Technol.* **2009**, *100*, 1007–1010.
(6) Kim, J. W.; Mazza, G. Optimization of phosphoric acid catalyzed fractionation and enzymatic digestibility of flax shives. *Ind. Crop Prod.* **2008**, *28*, 346–355.
(7) Moxley, G.; Zhu, Z.; Zhang, Y.-H. P. Efficient sugar release by the cellulose solvent-based lignocellulose fractionation technology and enzymatic cellulose hydrolysis. *J. Agric. Food Chem.* **2008**, *56*, 7885–7890.

(8) van Wyk, J. P. H.; Mohulatsi, M. Biodegradation of wastepaper by cellulase from *Trichoderma viride*. *Bioresour. Technol.* **2003**, *86*, 21–23.
(9) Imai, M.; Ikari, K.; Suzuki, I. High-performance hydrolysis of cellulose using mixed cellulase species and ultrasonication pretreatment. *Biochem. Eng. J.* **2004**, *17*, 79–83.
(10) Lin, J.; Chang, Y.; Hsu, Y. Degradation of cotton cellulose treated with hydrochloric acid either in water or in ethanol. *Food Hydrocolloids* **2009**, *23*, 1548–1553.
(11) Nada, A. M. A.; Hassan, M. L. Thermal behavior of cellulose and some cellulose derivatives. *Polym. Degrad. Stab.* **2000**, *67*, 111–115.
(12) Knill, C. J.; Kennedy, J. F. Degradation of cellulose under alkaline conditions. *Carbohyd. Polym.* **2003**, *51*, 281–300.
(13) Varma, A. J.; Kulkarni, M. P. Oxidation of cellulose under controlled conditions. *Polym. Degrad. Stab.* **2002**, *77*, 25–27.
(14) Wang, N.; Ding, E.; Cheng, R. Thermal degradation behaviors of spherical cellulose nanocrystals with sulfate groups. *Polymer* **2007**, *48*, 3486–3493.
(15) Varmat, A. J.; Chavan, V. B. A study of crystallinity changes in oxidized celluloses. *Polym. Degrad. Stab.* **1995**, *49*, 245–250.
(16) Varma, A. J.; Chavan, V. B.; Rajmohanan, P. R.; Ganapathy, S. Some observation on the high resolution solid state CP-MAS $^{13}$C-NMR spectra of periodate-oxidised cellulose. *Polym. Degrad. Stab.* **1997**, *58*, 257–260.
(17) Tian, C. M.; Xie, J. X.; Guo, H. Z.; Xu, J. Z. The effect of metal ions on thermal oxidative degradation of cotton cellulose ammonium phosphate. *J. Therm. Anal. Calorim.* **2003**, *73*, 827–834.
(18) Tian, C. M.; Guo, H. Z.; Zhang, H. Y.; Xu, J. Z.; Shi, J. R. Study on the thermal degradation of cotton cellulose ammonium phosphate and its metal complexes. *Thermochim. Acta* **1995**, *253*, 243–251.
(19) Devallencourt, C.; Saiter, J. M.; Capitaine, D. Characterization of recycled celluloses: thermogravimetry/Fourier transform infra-red coupling and thermogravimetry investigations. *Polym. Degrad. Stab.* **1996**, *52*, 327–334.
(20) Scheirs, J.; Camino, G.; Tumiatti, W. Overview of water evolution during the thermal degradation of cellulose. *Eur. Polym. J.* **2001**, *37*, 933–942.
(21) Sykes, P. *A Guidebook to mechanism in Organic Chemistry*, 6th ed; Person Education: Hallow, U.K., 1996.
(22) Kawamoto, H.; Hatanaka, W.; Saka, S. Thermochemical conversion of cellulose in polar solvent (sulfolane) into levoglucosan and other low molecular-weight substances. *J. Anal. Appl. Pyrol.* **2003**, *70*, 303–313.
(23) El Seoud, O. A.; Fidale, L. C.; Ruiz, N.; D'Almeida, M. L. O.; Frollini, E. Cellulose swelling by protic solvents: which properties of the biopolymer and the solvent matter? *Cellulose* **2008**, *15*, 371–392.
(24) Jin, H.; Zha, C.; Gu, L. Direct dissolution of cellulose in NaOH/thiourea/urea aqueous solution. *Carbohydr. Res.* **2007**, *342*, 851–858.
(25) Viet, D.; Beck-Candanedo, S.; Gray, D. G. Dispersion of cellulose nanocrystals in polar organic solvents. *Cellulose* **2007**, *14*, 109–113.
(26) Frey, M. W.; Li, L.; Xiao, M.; Gould, T. Dissolution of cellulose in ethylene diamine/salt solvent systems. *Cellulose* **2006**, *13*, 147–155.
(27) Fischer, S.; Leipner, H.; Thümmler, K.; Brendler, E.; Peters, J. Inorganic molten salts as solvents for cellulose. *Cellulose* **2003**, *10*, 227–236.
(28) Michael, M.; Ibbett, R. N.; Howarth, O. W. Interaction of cellulose with amine oxide solvents. *Cellulose* **2000**, *7*, 21–33.
(29) Zhao, H.; Kwak, J. H.; Wang, Y.; Franz, J. A.; White, J. M.; Holladay, J. E. Interactions between cellulose and *N*-methylmorpholine-*N*-oxide. *Carbohydr. Polym.* **2007**, *67*, 97–103.
(30) Dogan, H.; Hilmioglu, N. D. Dissolution of cellulose with NMMO by microwave heating. *Carbohydr. Polym.* **2009**, *75*, 90–94.
(31) Li, H.; Kim, N.-J.; Jiang, M.; Kang, J. W.; Chang, H. N. Simultaneous saccharification and fermentation of lignocellulosic residues pretreated with phosphoric acid-acetone for bioethanol production. *Bioresour. Technol.* **2009**, *100*, 3245–3251.
(32) Gebus, S.; Leiviskä, K. Knowledge acquisition for decision support systems on an electronic assembly line. *Expert Syst. Appl.* **2009**, *36*, 93–101.
(33) Kimmich, R.; Anoardo, E. Field-cycling NMR relaxometry. *Prog. Nucl. Magn. Reson. Spectrosc.* **2004**, *44*, 257–320.
(34) Lauffer, R. B. Paramagnetic metal complexes as water proton relaxation agents for NMR imaging: theory and design. *Chem. Rev.* **1987**, *87*, 901–927.
(35) Kiihne, S.; Bryant, R. G. Protein-bound water molecule counting by resolution of $^{1}$H spin−lattice relaxation mechanism. *Biophys. J.* **2000**, *78*, 2163–2169.
(36) Akira, I. NMR analysis of cellulose dissolved in aqueous NaOH solutions. *Cellulose* **1997**, *4*, 99–107.
(37) Moulthrop, J. S.; Swatloski, R. P.; Moyna, G.; Rogers, R. D. High-resolution $^{13}$C NMR studies of cellulose and cellulose oligomers in ionic liquid solutions. *Chem. Commun.* **2005**, *12*, 1557–1559.
(38) Conte, P.; Smejkalova, D.; Piccolo, A.; Spaccini, R. Evaluation of the factors affecting direct polarization solid state $^{31}$P-NMR spectroscopy of bulk soils. *Eur. J. Soil Sci.* **2008**, *59*, 584–591.
(39) Bertini, I.; Luchinat, C. *NMR of Paramagnetic Molecules in Biological Systems*; Physical Bioinorganic Chemistry Series; Lever, A. B. P., Gray, H. B., Deries, Eds.; Benjamin/Cummings Publishing: CA, 1986.
(40) Bakhmutov, V. I. *Pratical NMR Relaxation for Chemists*; Wiley: Chichester, U.K., 2005.
(41) Jóhannesson, H.; Denisov, V. P.; Halle, B. Dimethyl sulfoxide binding to globular proteins: a nuclear magnetic relaxation dispersion study. *Protein Sci.* **1997**, *6*, 1756–1763.
(42) Conte, P.; Bubici, S.; Palazzolo, E.; Alonzo, G. Solid state $^{1}$H-NMR relaxation properties of the fruit of a wild relative of eggplant at different proton Larmor frequencies. *Spectrosc. Lett.* **2009**, *42*, 235–239.

**Received June 26, 2009. Revised manuscript received August 28, 2009. Accepted September 3, 2009. This work was partially funded by CE.R.T.A. s.c.r.l. (Centri Regionali per le Tecnologie Alimentari; http://www.certa.it/default.asp).**